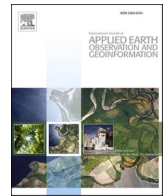




Contents lists available at ScienceDirect

International Journal of Applied Earth Observations and Geoinformation

journal homepage: www.elsevier.com/locate/jag

Land uplift linked to managed aquifer recharge in the Perth Basin, Australia

A.L. Parker^a, J.-P. Pigois^b, M.S. Filmer^a, W.E. Featherstone^{a,*}, N.E. Timms^a, N.T. Penna^c^a School of Earth and Planetary Sciences and The Institute for Geoscience Research, Curtin University of Technology, GPO Box U1987, Perth, WA 6845, Australia^b Department of Water and Environmental Regulation, 7 Ellam Street, Victoria Park, WA 6100, Australia^c School of Engineering, Newcastle University, Newcastle upon Tyne, NE1 7RU, UK

ARTICLE INFO

Keywords:

InSAR
TerraSAR-X
Managed aquifer recharge
Vertical land motion
Groundwater management
Land uplift

ABSTRACT

While the link between groundwater extraction and land subsidence is well documented, observations of land uplift associated with groundwater replenishment are less so. In the Perth Basin, Western Australia, a programme of managed aquifer recharge (MAR) commenced in August 2017 and is designed to sustain levels of hydraulic head in aquifers valuable for extraction. Space-based TerraSAR-X satellite radar measurements were used to capture the first 3.5 years of MAR, providing an insight into the evolution of ground uplift in the Perth Basin that is spatially and temporally related to the MAR injection volumes and the injection-induced changes in hydraulic head. Significantly, the X-band InSAR has spatial coverage around the single injection point, and the time series begins prior to the start of the injection, rather than a generalised study of ground surface and aquifer change from multiple groundwater recharge contributions. This enables the observed ground uplift to be correlated with the time of initial injection, pause, then resumption with increased volumes. The X-band InSAR identified maximum displacements of up to 20 ± 3 mm in the vicinity of the injection bores, but which subside when injection is paused. The spread of displacements from the injection site extends over 14 km southwards with the dispersion pattern identifying linear boundaries that sharply delineate displacements in the north-west and north-east. The extent of the region impacted by ground uplift is likely linked to the distribution of extraction bores and heterogeneities in the subsurface geology, including a persistent linear feature that has not yet been considered in hydrogeological models of the region. This article focusses on the immediate surface response to the MAR injection, and identifying the constraining physical features for the injected recharge, thus providing an additional insight into the challenging and complex Perth Basin. It also demonstrates the millimetric accuracy possible from X-band radar satellites that permits MAR volumes to be managed to avoid infrastructure damage that may undermine public confidence in the MAR program.

1. Introduction

Mid-latitude population centres with semi-arid, Mediterranean-type climates, such as Perth, Western Australia (WA; Fig. 1), are projected to experience the greatest impacts of climate change upon renewable water resources (IPCC, 2007). In response to reduced rainfall and an increasing population, Perth, like many other cities, has become increasingly reliant upon subsurface groundwater extraction (McFarlane et al., 2012). To sustain water levels in areas that are of high value for extraction, Perth's principal supplier of water, the Water Corporation of WA, has commenced groundwater replenishment via injection of recycled, treated-to-be-potable wastewater into two major mostly confined subsurface aquifers in the Perth Basin: Leederville and Yarragadee. This managed aquifer recharge (MAR) was commissioned in August 2017 to

address increasing demand for water and less rainfall (Water Corporation, 2009).

Changes in groundwater levels within subsurface aquifers alter the effective stress of the overburden, often resulting in ground displacements that are measurable at the Earth's surface (Poland and Ireland, 1988). Surface displacements are related to geo-mechanical properties of the aquifer system (e.g., aquitard thickness) and land-surface displacement measurements can be used as a proxy to constrain changes in hydraulic head (the level of groundwater within an artesian monitoring bore). The link between groundwater extraction and subsidence (sinking of the ground) has been observed in cities and agricultural regions globally (e.g., Galloway and Burbey, 2011). Long-term, irrecoverable subsidence is associated with inelastic compaction of aquifers (e.g., Galloway and Burbey, 2011). In Perth, long-term

* Corresponding author.

E-mail address: W.Featherstone@curtin.edu.au (W.E. Featherstone).

<https://doi.org/10.1016/j.jag.2021.102637>

Received 6 June 2021; Received in revised form 11 November 2021; Accepted 21 November 2021

Available online 1 December 2021

0303-2434/© 2021 Published by Elsevier B.V. This is an open access article under the CC BY-NC-ND license (<http://creativecommons.org/licenses/by-nc-nd/4.0/>).

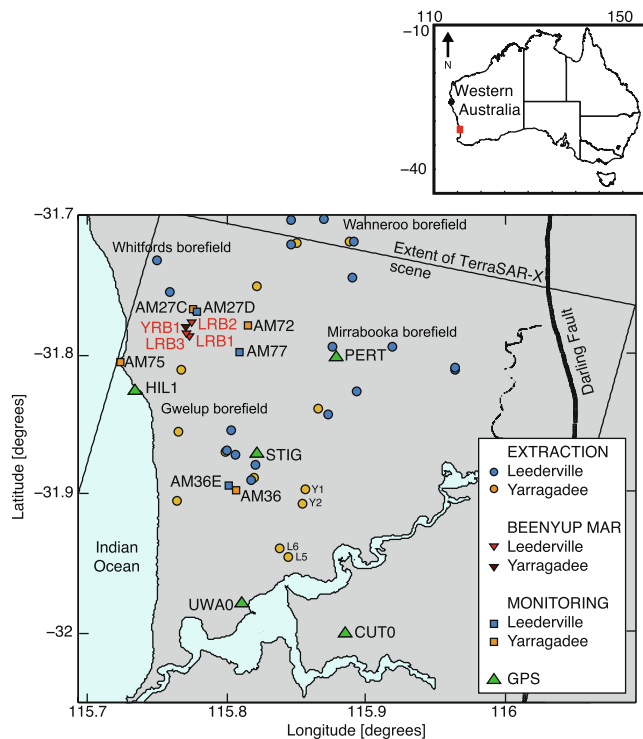


Fig. 1. Map of the Perth metropolitan region showing the location of datasets used in this study. Labelled are extraction bores (circles), injection bores (inverted triangles) and a subset of monitoring bores (squares) for the two major aquifers in the Perth Basin: Leederville and the deeper Yarragadee. Continuously operating GPS stations (green triangles) are also shown. Inset: Map of Australia with the study region shown by the red rectangle. (For interpretation of the references to colour in this figure legend, the reader is referred to the web version of this article.)

subsidence of between $\sim 3\text{--}6$ mm/yr since the 1970s and 1990s has been observed from continuously operating Global Positioning System (GPS) instruments (Featherstone et al. 2015 and the references therein), repeated differential levelling (Lyon et al., 2018) and Interferometric Synthetic Aperture Radar (InSAR: Parker et al., 2017). This long-term subsidence is not discussed further here. Geodetic observations also show non-linear secular trends correlated with changed rates of groundwater extraction, superposed by a seasonal signal that is correlated with near-surface geology and expansive soils (Lyon et al., 2018).

The opposite phenomenon - land uplift due to increases in groundwater levels - is much less frequently observed and reported (e.g., Teatini et al., 2011; Sneed and Brandt 2020; Brandt et al. 2020; Neely et al. 2021), and not previously reported where the uplift is directly related in time and space to the start of a single MAR injection point. The commissioning of MAR in the Perth Basin therefore provides an opportunity to capture the onset of wastewater injection into confined and compacted aquifer systems. We use X-band InSAR to provide spatially and temporally dense observations of the surface response to MAR between 25 December 2016 and 27 December 2020 (we use decimal years from hereon: 2016.98 – 2020.99, selecting an integer number of years to average out the seasonal signals).

The focus of this study is therefore to specifically examine the spatial and temporal evolution of land surface response to MAR over the first ~ 3.5 years of its operation (2017.67 – 2020.98). The injection program over this initial time includes three distinct phases, where injection volumes increase, then temporarily cease (Fig. 2). These variations in volume, and temporary pauses during these three stages allow an insight into (1) the ability of X-band InSAR to detect mm-level ground surface variations in time, (2) the presence of barriers to groundwater flows for two of the major aquifers in the Perth Basin: the Leederville and the

deeper Yarragadee aquifers, and (3) the initial ground surface response from the start of a MAR program.

While there are other studies that use InSAR to monitor land surface displacement that include the effects of MAR, none appear to specifically measure displacement at and around the injection point during the period where the injection is started and paused, with different volumes during the injection period. For example, Sneed and Bandt (2020) use InSAR (C-band from ERS1/2, Envisat and Sentinel-1; Sneed et al., 2014; Brandt et al., 2020) from 1995 to 2017 in the Coachella Valley, California, USA to review increases in aquifer-wide groundwater levels following recharge from a combination of groundwater substitution, conservation and multiple MAR facilities. On the other hand, Neely et al. (2021) use C-band Sentinel-1 to focus on uplift from natural recharge and reduction in groundwater pumping (extraction), relating this to patterns of seasonal amplitude. In that study, Neely et al. (2021) uplift is considered seasonal rather than directly attributable to MAR. Castellazzi and Schmid (2021) identify the uplift in the Perth Basin using Sentinel-1 C-band and make the link to the Beenyp MAR, but do not analyse its evolution and variability over four years, showing only the displacement rate for the period of observation for ~ 1 year from August 2017 to August 2018.

Our findings will contribute to an understanding of the direct effects of MAR on the land surface, including structural controls on groundwater flow, so as to optimise the injection of waste water to subsurface aquifers without causing surface infrastructure damage from uplift that may undermine public confidence in the program.

2. Perth Basin groundwater and datasets

The city of Perth is located on the Swan Coastal Plain in the central portion of the sedimentary Perth Basin, bound to the east by the steeply-dipping Darling Fault and the west by the Indian Ocean (Playford et al., 1976; Lambeck, 1987; Fig. 1). In the vicinity of Perth, the sedimentary succession houses two major mostly confined aquifers: Leederville (depths of $\sim 50\text{--}300$ m) and the larger (up to 2 km thick), deeper Yarragadee (Davidson and Yu, 2008; Olierook et al., 2015). Both aquifers consist of laterally discontinuous siltstones, sandstones and shales, and are overlain by the unconfined, superficial aquifer (e.g., Timms et al., 2015).

Monthly averages of extracted groundwater were obtained from the Water Corporation of WA (Fig. 2). The Water Corporation began extraction from the Leederville and Yarragadee aquifers in the mid-1970s. Rates increased between 1990 and 2005 with the installation of five new production bores (Featherstone et al., 2015), four of which are located in the Gwelup borefield (see location in Fig. 1). During this study period the largest extraction volumes occur in the Gwelup borefield (Fig. 2C). Extracted volumes at all bores vary seasonally, peaking during the Southern Hemisphere summer (Fig. 2).

Natural recharge of the Perth Basin aquifers occurs from rainfall, mostly between May - October (Fig. 2). MAR into the Leederville and Yarragadee aquifers occurs at the Beenyp wastewater treatment plant (Fig. 1). First, the wastewater is treated to a potable standard. Injection then takes place through four bores (red triangles in Fig. 1): three at depths between ~ 125 m – 235 m below ground level into the Leederville aquifer (LRB1, LRB2, LRB3); and one at a depth between $\sim 390\text{--}745$ m below ground level into the Yarragadee aquifer (YRB1). During the first 3.5 years of operation, MAR has occurred in three stages (labelled stages 1–3 in Fig. 2 and thereafter). Each injection bore is accompanied by a monitoring bore to measure changes in hydraulic head and water quality directly at the injection site. Injection volumes and hydraulic head levels at the monitoring bores were provided by the Water Corporation of WA.

An array of artesian monitoring bores in the Perth Basin provides measurements of hydraulic head on a monthly, quarterly or daily basis. Records were accessed from the Department of Water and Environmental Regulation's Water Information Reporting Service (<http://wir>.

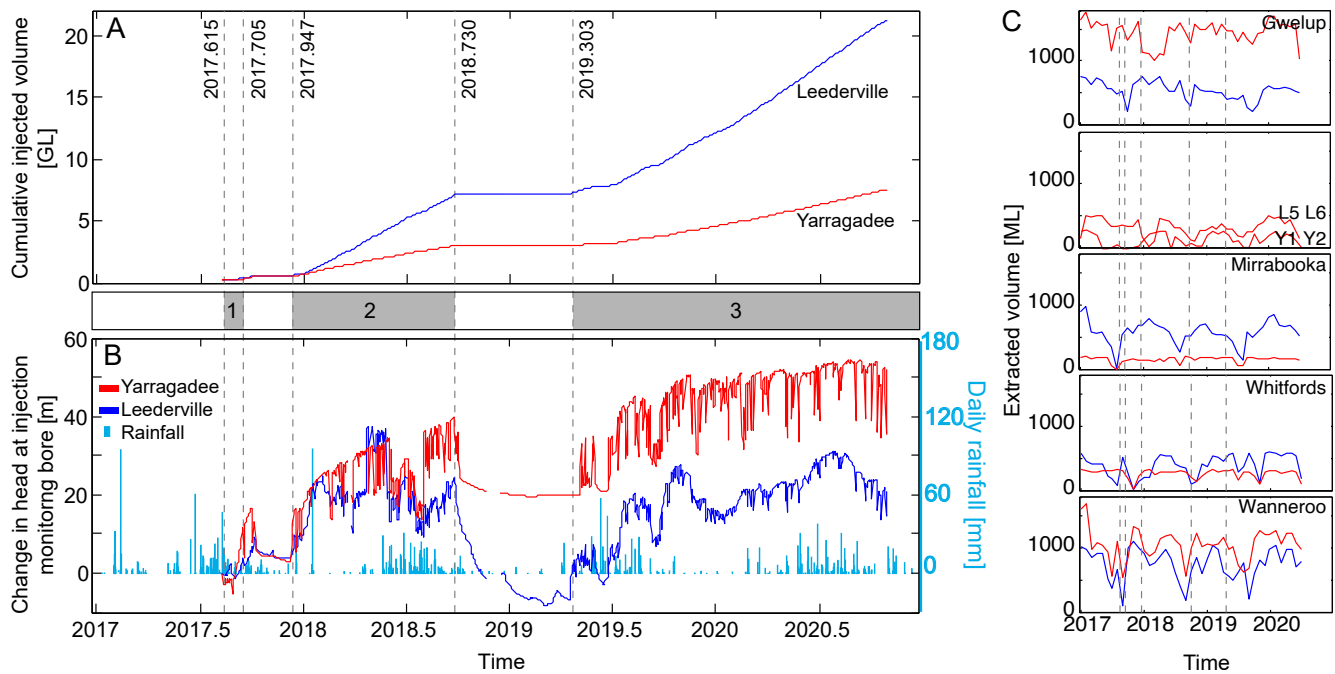


Fig. 2. Time series of groundwater extraction and injection. Locations of extraction and injection bores are shown in Fig. 1. A) Cumulative injection volume for the Leederville (LRB1, LRB2, LRB3) and Yarragadee (YRB1) injection bores. Injection occurred in three stages as shown by the vertical timelines. Labelled dates and dashed lines in this and subsequent figures are TerraSAR-X data acquisitions closest to the start/end of the stages. B) Change in hydraulic head measured in monitoring wells adjacent to injection bores. Leederville (blue) is the average of the change measured in LRB1, LRB2 and LRB3. Light blue shows daily rainfall levels above 0 mm (Bureau of Meteorology: <http://www.bom.gov.au/climate/dwo/IDCJDW6111.latest.shtml> accessed on 26 April 2021). C) Time series of groundwater extraction in the study region. Time series for each aquifer - Leederville (blue), Yarragadee (red), - are the total extracted volume from all bores in each borefield. Extraction and injection data is provided by the Water Corporation of WA. (For interpretation of the references to colour in this figure legend, the reader is referred to the web version of this article.)

water.wa.gov.au/Pages/Water-Information-Reporting.aspx, accessed on 29 April 2021). We use bores that are either quality-controlled and used to calibrate the Perth Regional Aquifer Modelling System (Davidson and Yu, 2008; De Silva et al., 2013; AM27C, AM27D) or that have been drilled as part of a recent re-interpretation of the Perth aquifer system and to monitor the aquifer responses to reinjection at Beenyp (DWER, 2021; AM72, AM75, AM77).

3. Geodetic data and processing methods

3.1. Interferometric Synthetic Aperture radar

Space-based InSAR provides high spatial resolution (reaching sub-metre), large-scale (tens of kilometres) maps of surface displacements, known as interferograms, by comparing the phase of successive Synthetic Aperture Radar (SAR) satellite images. Assuming the phase-change contribution from the satellite orbit and topography are removed, the remaining interferogram phase-changes, measured in multiples of the satellite wavelength, are primarily due to displacements of the Earth's surface plus variations in the refractivity of the atmosphere (Massonnet et al., 1993; Bürgmann et al., 2000). InSAR can be used as a tool for deriving head change measurements that are spatially denser and cover a larger area than discrete borehole records (e.g., Reeves et al., 2011; Chen et al., 2016), and for delineating hydro-geological features and structures within a groundwater basin (cf., Lu and Danskin, 2001; Chaussard et al., 2014).

In this study, we use 119 X-band (wavelength ~ 31 mm) TerraSAR-X stripmap images provided by the German Aerospace Center (DLR) spanning 2016.98 to 2020.99 and separated (mostly) by 11-day intervals. This time period is selected to provide four integer years of data to reduce seasonal effects, which are shown to be large in a previous InSAR study of this region (Parker et al., 2017). From these SAR images,

we formed 455 small baseline (SBAS) interferograms processed as described in Filmer et al. (2020), using the small baseline multi-temporal InSAR method in the Stanford Method of Persistent Scatterers software (StaMPS; Hooper et al., 2007) and a 1 arc sec (~ 30 m) Shuttle Radar Topographic Mission (SRTM) digital surface model (Farr et al., 2007). Long-wavelength orbital and ionospheric effects were removed using a phase ramp, justified by the small scene extent of $\sim 30 \times 40$ km (Hooper et al., 2007) and relatively low sensitivity of X-band to ionospheric effects (Gomba et al., 2017).

Non-systematic atmospheric phase delays were reduced by the number of interferograms (455) used in the analysis and application of a 33-day temporal filter within StaMPS processing. The resulting interferograms were resampled from ~ 3 m spatial resolution to a $30 \text{ m} \times 30 \text{ m}$ grid so as to reduce the processing time and smooth noisy pixels. Rather than using a single reference pixel, we reference the measurements to the mean phase of all pixels (e.g., Finnegan et al., 2008) located outside the zone impacted by water injection (i.e., east of longitude 115.9°E). InSAR displacements are therefore measured relative to this region. Line of sight phase values (in radians) were converted to vertical displacements (in millimetres) using the heading and incidence angle of the satellite (e.g., Wright et al., 2004) under the assumption that all displacement occurs in the vertical direction (cf. Parker et al., 2017; Chaussard and Farr, 2019). Time series of cumulative displacements are computed using a least-squares approach (Berardino et al., 2002). Cumulative displacement maps are then produced at each TerraSAR-X acquisition epoch using the time series at each pixel.

3.2. GPS

To validate the ground surface displacements from InSAR, we use time series of daily vertical displacements at five continuously operating GPS installations in the Perth Basin (for locations, see Fig. 1). Of these

instruments, two are mounted on buildings (UWA0, CUT0), one is located on a marine jetty for tide-gauge monitoring (HIL1) and two are on deep-seated concrete pillars (STIG, PERT). All data are in the public domain with the exception of STIG, which is a commercially operated site.

The daily GPS data were processed using the GipsyX v1.6 software (Bertiger et al., 2020) in precise point positioning (PPP) mode, fixing ‘repro3’ Jet Propulsion Laboratory final fiducial-free precise orbits and satellite clock parameters. The daily position estimates per station were concatenated to form the coordinate time series. Ambiguity-fixed positions were estimated daily using 24 h of data and transformed to the IGB14 reference frame. Parameter estimation and error modelling followed Blewitt et al. (2018). No spatial or temporal filter was applied.

4. Results

4.1. Comparison between InSAR and GPS results

We first compare the InSAR results with GPS for validation and to determine whether ground displacements linked to MAR are detected in the GPS time series. InSAR time series are calculated using all pixels located within 100 m of each GPS site, with the error bars in Fig. 3 representing one standard deviation of these values. We acknowledge that this is not a formally propagated error, but gives us an estimate of the variability in the precision of the InSAR measurements co-located with each GPS site. The 100 m radius was selected as an arbitrary limit. This choice is supported by tests conducted for Filmer et al. (2020) at Perth Basin GPS sites, finding that there was no significant difference in rates when the single nearest pixel was selected compared to using more pixels over a larger radius. Johnston et al. (2021) also found insignificant differences in rates between using a single pixel and a 70 m radius when connecting to GPS sites in a different study area (south eastern Australia) that was undergoing deformation. GPS time series show the PPP GPS position solution on the day of each SAR image acquisition. We convert the absolute GPS heights to relative heights by subtracting the epoch-zero, allowing us to present a clearer comparison

to the InSAR measurements. Variability in the time-series is attributed to the effects of seasonal rainfall on the shallow surface and, for the GPS, effects of the installation type including expansion and contraction of buildings.

It is significant that ground displacements linked to MAR are not detected in the GPS height time series (or the InSAR time series calculated at these same locations: Fig. 3). This suggests that the GPS sites are located outside the zone that is impacted by MAR and validates our choice of zero-reference for the interferogram phase (the mean of pixels east of 115.9°E). Had GPS alone been used in this investigation, no ground displacements linked to MAR would be detected. This highlights the importance of spatially-dense InSAR measurements

4.2. Spatial extent of displacements

The InSAR measurements provide a region-wide overview of ground displacements occurring during MAR. The main features of the displacements include: 1) maximum relative displacement of up to $\sim 20 \pm 3$ mm occurring at the Beenyup MAR site; 2) the spatial distributions of displacements from the injection site out to ~ 14 km southwards; and 3) linear boundaries that sharply delineate displacements in the north-west and north-east (Fig. 4B). These features are observed in each of the injection stages, with the magnitude of displacements decreasing between stages when injection is paused (see example of stage 2 in Fig. 4B). The temporal resolution of the X-band SAR is advantageous for capturing these time-dependent variations in magnitude. Error estimates for the TSX InSAR are shown in Fig. 3 and Fig. 5 for time series calculated at the GPS and monitoring bores, respectively. These indicate TerraSAR-X errors at these locations of ~ 2 mm and up to 5 mm for monitoring bore AM77, which is located close to the shore of a lake where pixels are sparse (Fig. 6). These TSX error estimates are comparable to those from Filmer et al. (2020). We discuss the geological controls upon these features in Section 5.

The zone of maximum displacements does not expand radially out from the site of injection, as would be expected for a homogeneous and tabular aquifer (Theis, 1935), but instead is dominated by spreading in

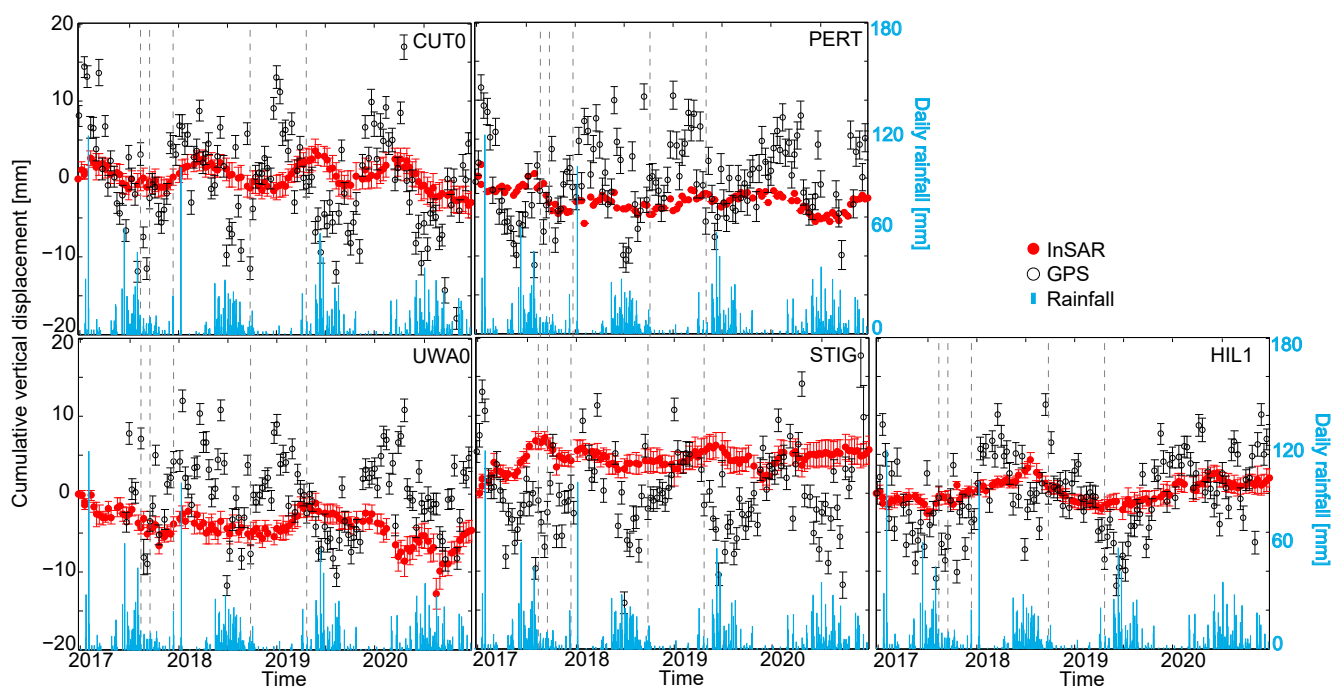


Fig. 3. Comparison between time series of vertical displacements from InSAR and GPS measurements. GPS locations are shown in Fig. 1. Error bars for GPS are one sigma formal errors (68% confidence), and for InSAR represent one standard deviation of all pixels within 100 m of the GPS location. Dashed vertical lines show injection phases as in Fig. 2.

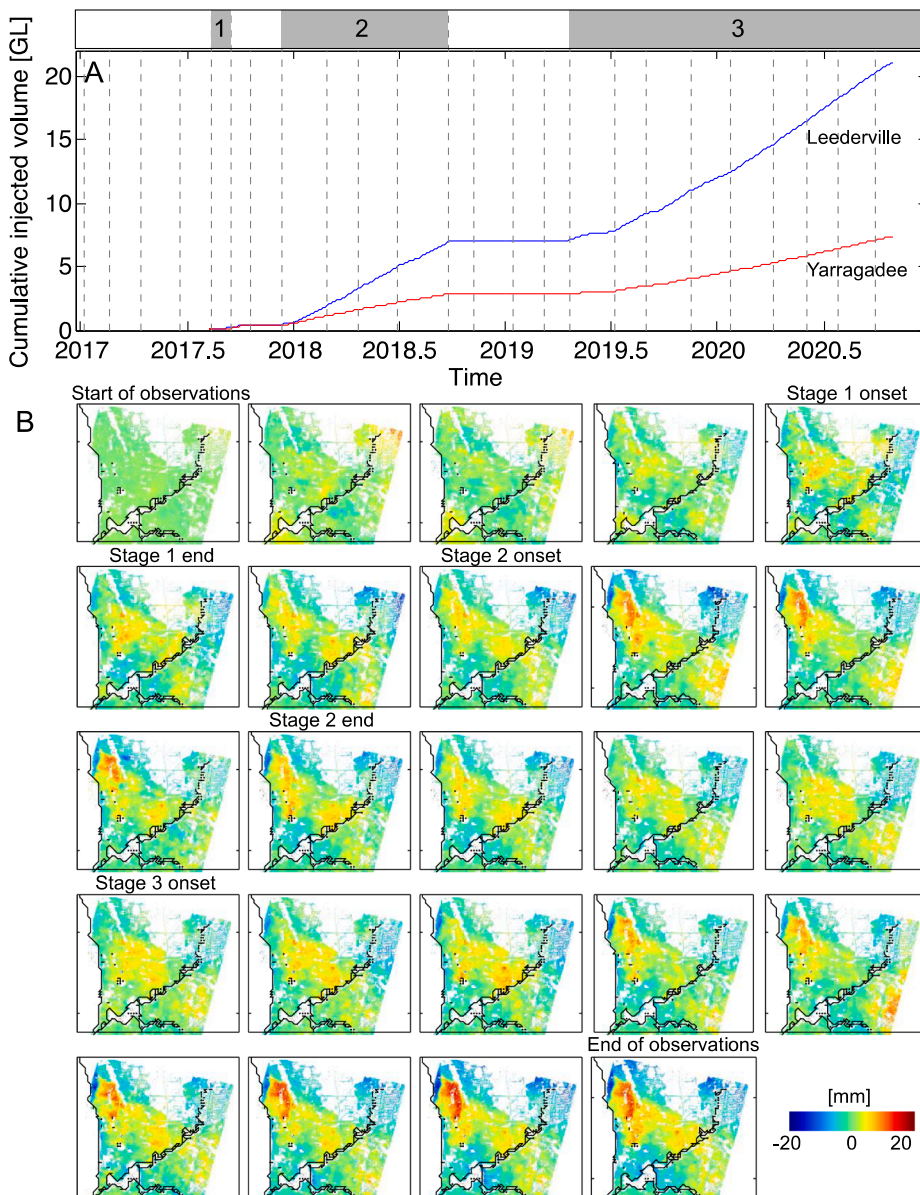


Fig. 4. Maps of cumulative ground displacements (vertical magnitude in mm) linked to different stages of MAR. A) Time series of the total injected volume as in Fig. 2. Dashed vertical lines show the dates of the displacement maps shown in B and are a subset of the TerraSAR-X acquisition epochs (every fifth TerraSAR-X acquisition includes the epochs closest to the start/end of each injection stage). B) Maps of cumulative displacements (relative to the first TerraSAR-X acquisition) showing the progression of ground displacements linked to MAR. Positive (red) indicates uplift. (For interpretation of the references to colour in this figure legend, the reader is referred to the web version of this article.)

an elongated region striking approximately NNW-SSE (Fig. 4B). The maximum uplift extends close to the coastline in the west. To the east, displacements become more diffuse further from the injection site, decreasing to < 5 mm in magnitude. To the south, displacements extend as far as Herdsman Lake (see circular pixel-free region at the southern extent of uplifted region in Fig. 4B). To the north, the terminus of the displacement field is marked by abrupt linear boundaries striking NNE-SSW and NW-SE that meet at acute angles defining the northernmost extent of displacements (Fig. 5B). This distinctive feature has been observed in other InSAR datasets covering this region and spanning different time periods (Parker et al., 2017; Castellazzi and Schmid, 2021), with the sign of displacements on one side of the boundary always observed to be opposite to that of displacements on the other. Across these boundaries displacement gradients are large, exceeding 15 mm per km.

4.3. Comparison between ground displacements and hydraulic head

We explore the features in Fig. 4 by jointly assessing ground displacements and groundwater information derived from monitoring

boreholes (for locations, see Fig. 1). The InSAR time series are generated using the same approach as in Section 4.1. Ground-surface displacements result from the total hydraulic head change and cannot be linked to individual aquifers.

Monitoring bores AM27D and AM27C are closest to the injection site (~ 1.2 km away), sampling the Leederville and Yarragadee aquifers, respectively. Time series of hydraulic head for both aquifers show step increases of 5–15 m associated with the onset of injection at each stage (Fig. 5A). When injection paused between stages, head levels decreased (cf. Theis, 1935). As AM27C and AM27D are located in close proximity to each other, time series of ground displacements at the two sites are almost identical (Fig. 5D). The short duration of stage 1, and interval between stages 1 and 2, means that displacements linked to these two stages cannot be separated. Instead, we observe a first peak of ~ 11 mm that occurs mid stage 2. Ground displacements then decreased as injection was paused (and natural recharge from seasonal rainfall also decreased), before increasing again during stage 3 to a similar magnitude (Fig. 5D).

There are monitoring bores that sample the Yarragadee aquifer located on both sides of the sharp north-western edge of the

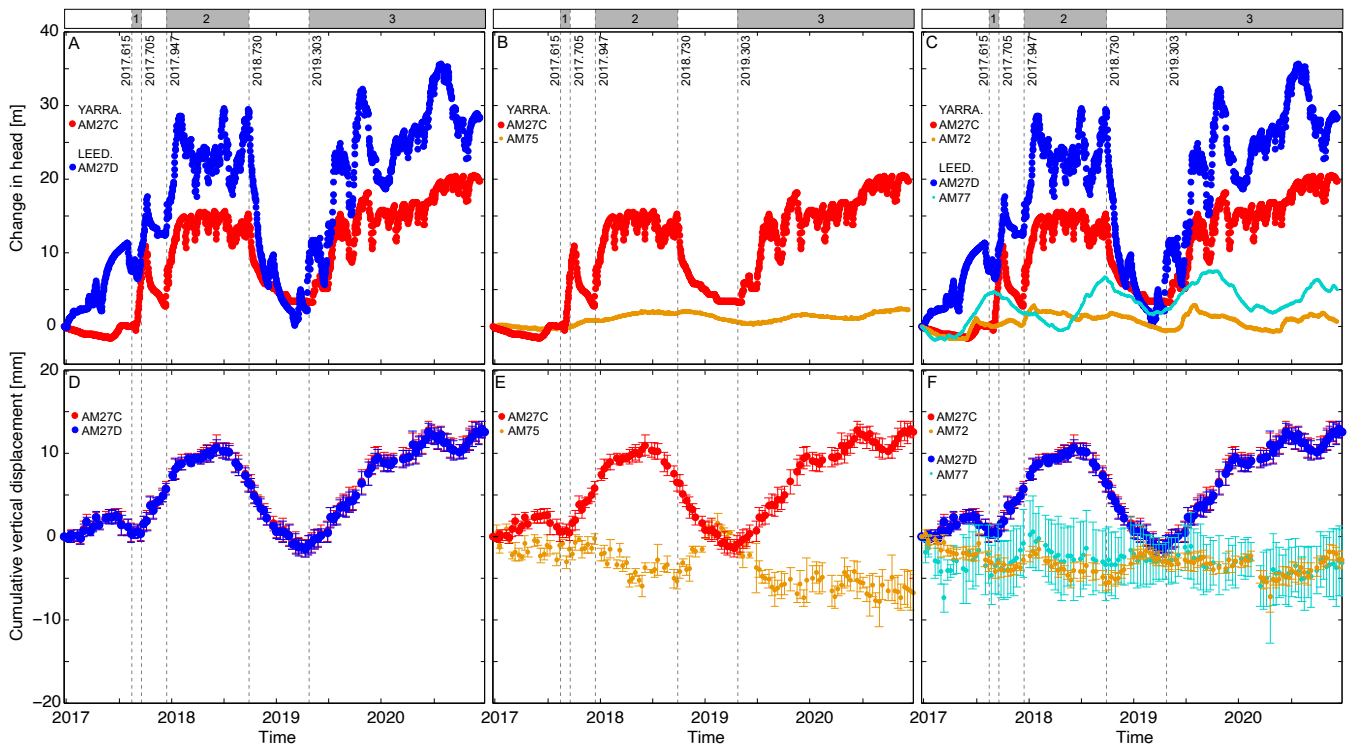


Fig. 5. Time series of hydraulic head at artesian monitoring bores and proximal ground displacements. Bore locations are shown in Fig. 1. A-C) Change in hydraulic head (measured in metres relative to head levels at the time of MAR onset) at artesian monitoring bores. D-F) Time series of cumulative vertical ground displacement measured (in mm) using TerraSAR-X at the location of the monitoring bores using the method described in Section 3.1. Dashed lines show the timing of injection stages 1–3 with TerraSAR-X epochs labelled as in Fig. 2.

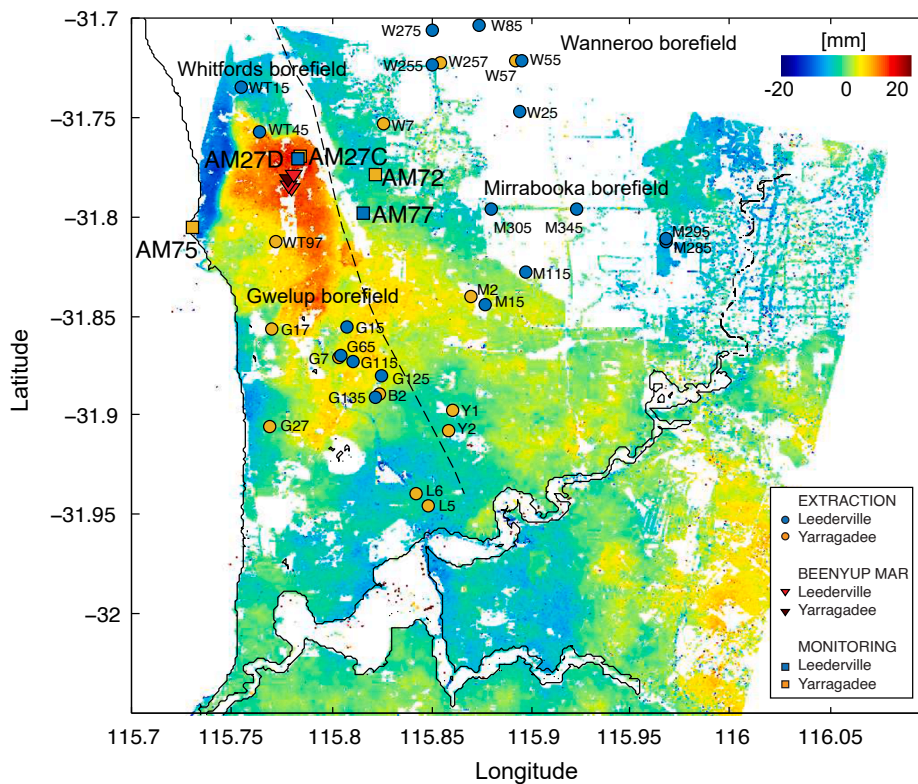


Fig. 6. Map of maximum cumulative ground displacements since 2016.9822 and the location of monitoring and extraction bores. Extraction, injection and monitoring bores are as in Fig. 1. Dashed line is a subsurface structure inferred from De Silva et al. (2013).

displacement field described in Section 4.2. Bore AM27C is located in the zone of maximum relative uplift, whereas bore AM75 is located on the region of apparent subsidence (negative relative ground displacement) to the west of this boundary (Fig. 6). As before, AM27C records step increases in hydraulic head during each injection stage. Conversely, AM75 records < 3 m variation throughout the observation period (Fig. 5B), indicating that there is a hydraulic barrier (aquitard) between these two locations. These differences are also observed in the TerraSAR-X ground displacement time series (Fig. 5E). Whereas the location of AM27C exhibits uplift during injection stages, the location of AM75 undergoes subsidence of ~7 mm throughout the observation period with the exception of a period of uplift that corresponds to the pause in injection between stages 2 and 3, during which AM27C subsided.

At the north-eastern extent of the uplifted region, similar observations can be made. A steep displacement gradient is observed and monitoring bores for both the Leederville (AM27D, AM77) and Yarragadee (AM27C, AM72) aquifers are available on either side of this sharp gradient in displacement magnitude (Fig. 6). Hydraulic head measured at artesian monitoring bore AM27 in both the Leederville (AM27D) and Yarragadee (AM27C) aquifers closely mirrors that measured at the injection monitoring bores.

At AM77, hydraulic head levels in the Leederville aquifer to the east of the boundary show a seasonal variation correlating with increases in rainfall that is not altered by injection and that is comparable to seasonal variations measured at other bores in the basin (Fig. 5C). Similarly, the Yarragadee aquifer monitoring bore located on the eastern side of the boundary (AM72) demonstrates no significant change in head (Fig. 5C). The maximum increase in head, which occurs at the onset of Stage 3, is < 5 m and is similar in magnitude to other perturbations seen in the time series. Ground displacement time series show similar results, with overall subsidence of 1–2 mm observed east of this boundary (Fig. 5F).

5. Discussion

5.1. Influences on the spatial extent of ground displacements

The observations made here using X-band InSAR demonstrate that relative ground displacements occurring during periods of MAR do not spread radially around the injection site, as could be expected from a simple aquifer geometry with homogeneous properties (cf. Theis, 1935). Instead, the most uplifted domain defines an elongated region striking approximately NNW-SSE, bound to the north by abrupt linear features. Factors that likely contribute to the spatial extent of ground displacements arising from MAR include 1) the location of bores extracting groundwater; and 2) heterogeneities within the subsurface geology.

The Gwelup extraction borefield (shown in Fig. 2B to extract the largest volumes of groundwater over the observation period) is located directly to the south of the injection site (Fig. 6). Extraction in this region acts as a groundwater sink, resulting in a preferential path for the injected groundwater towards the extraction bores. Other borefields may be located too close (Whitfords) or too far away (e.g., Wanneroo and Mirrabooka) from the Beenyup injection site to have a measurable effect upon ground displacements within our observation period.

Heterogeneities in the subsurface that may impact the extent of uplift include: variations in the lateral extent and thickness of the aquifers, reflecting the primary depositional geometry and any subsequent local/regional erosion and/or consequent juxtaposition with other aquifers and aquitards; faulting and related hydraulic compartmentalisation related to formation juxtaposition and fault damage-related changes in rock properties; large scale, systematic intra-formational lateral variations in rock properties; and/or pre-existing hydrogeological factors, such as localised hydraulic head or pressure variations.

Existing hydrogeological models of the study region are largely constrained by sparse borehole data (Davidson and Yu, 2008). Given the high spatial and temporal resolution of the X-band InSAR measurements and large spatial uncertainties upon features of these models, it is

difficult to directly link the InSAR-derived land surface displacement to the subsurface geology. However, we propose that the following are considerations worthy of further investigation:

- At the southern terminus of uplift (-31.91° S, 115.80° W; Fig. 6), hydrogeological models propose that the Cretaceous sediments of the Leederville Formation (that house the Leederville aquifer) were eroded away and replaced by the King's Park Formation (Davidson and Yu, 2008). As most MAR occurs into the Leederville aquifer (Fig. 2), the occurrence of the King's Park Formation, and absence of the Leederville Formation, is likely to be a control upon the southern extent of ground displacements.
- Geophysical methods and geological mapping have been used to infer fault geometries in the study region (e.g., Corbel et al., 2012). Both NNE- and NNW-trending faults were inferred in the Perth metropolitan area by Timms et al. (2012) from topographic scarps and gravity anomalies. However, none of the inferred faults in their survey area (which did not extend as far north as our study area) coincide with the observed gradients in measured ground displacements. Furthermore, no existing studies map a discontinuity in the vicinity or in the same orientation as the sharp north-western boundary of ground displacements observed in this and other studies. In fact, previously inferred fault geometries generally trend approximately perpendicular to this feature.
- The north-eastern boundary of uplift (Section 4.2; Figs. 5, 6) is coincident with a fault-like feature inferred from pump tests (De Silva et al., 2013; dashed line in Fig. 6) and linked to a slowing of groundwater flow between Yarragadee aquifer monitoring bores AM27C and AM72 (Clohessy, 2017). The characteristics of this feature (i.e., whether it is a fault or a zone of low connectivity) and the effects upon groundwater flow, including aquifer compartmentalisation, are not well defined. However, its location in the primary zone of groundwater extraction and injection means that further understanding is required. Notwithstanding, this study demonstrates that X-band InSAR observations of the land surface response to MAR provide a unique insight to help understand this and other features of the subsurface geology that impact upon the Perth Basin groundwater system that cannot be achieved at the required spatial or temporal scales by existing terrestrial measurement techniques.

5.2. Implications for future monitoring and groundwater management

To avoid negative effects of MAR and sustain public confidence, MAR operations require monitoring of water quality, movement of the injected water, any changes to the groundwater system and surface land displacement that could damage public or private infrastructure. Here, InSAR measurements are used to track the spatial and temporal development of land uplift arising from the injection of treated wastewater. This approach is a cost-effective way to monitor aquifer-scale hydraulic head changes caused by the injection or extraction of water. Consequently, space-based geodetic measurements of aquifer systems are shown to be valuable inputs for water management strategies (e.g., in the Santa Clara Valley, California: Chaussard et al., 2017; the Coachella Valley, California: Sneed and Brandt, 2020; and the San Joaquin Valley, California: Neely et al., 2021). These spatially dense surface displacement measurements can also be used to inform decisions about the location of future monitoring, extraction and injection bores.

Our observations are significant in that they directly map the ground surface response specifically to the MAR, from the initial injection, and through three stages with variable injection volumes and complete pauses between each stage. These focussed results from the Perth Basin reveal sharp linear features that bound the area impacted by ground displacements, and are significant for future investigations of the potential for compartmentalisation of the aquifer in high-value areas of extraction. Using InSAR observation of MAR to identify faults or other barriers to flow is also significant for geothermal exploration and CO₂

sequestration in the Perth Basin (Corbel et al., 2012; Timms et al., 2012). Groundwater extraction and injection activities are associated with the activation of pre-existing shallow faults, and induced microseismic/seismic events due to the impacts upon local stress regimes (Gambolati and Teatini, 2015 and the references therein).

However, and importantly, we emphasise that we are not predicting an increased probability of seismic activity in the Perth Basin due to groundwater extraction or MAR. Furthermore, our observations suggest that previously inferred faults - if they indeed exist - have not significantly compartmentalised ground displacements in the Perth metropolitan area over the duration of this study, either by being activated or acting as permeability barriers. Nevertheless, sharp linear gradients in ground displacement could indicate the presence of previously unidentified faults or other permeability barriers in the northwest of the study area that are important for groundwater flow over timescales of this study.

Most other examples of uplift related to fluid injection in the literature describe hydrocarbon production – with fluid either injected to stimulate production or to counteract subsidence caused by hydrocarbon extraction (Gambolati and Teatini, 2015). In other cases involving MAR, the studies have focussed on aquifer-wide stabilisation of groundwater levels and land surface subsidence due to groundwater extraction, rather than a specific evaluation of the initial stages of injection at a MAR facility and the direct response of the land surface. In Perth, continued monitoring of ground displacements occurring coincident with MAR is significant to understand any potential negative impacts on infrastructure. Further monitoring, which will include the newly installed continuous GPS and SAR corner reflector at the Beenyup injection site, will also determine the impact of recharge upon long-term inelastic compaction of the aquifer system (e.g., Bell et al., 2008) that has been linked to subsidence of the Perth Basin since the 2000s (Featherstone et al., 2015).

6. Conclusions

Artificial recharge of aquifers (MAR) in the Perth Basin with treated wastewater has directly resulted in up to 20 ± 3 mm of uplift during the first 3.5 years of MAR operations at a single injection site. Space-based InSAR provides the only set of observations that is spatially and temporally dense enough to monitor ground displacements linked to injection-induced changes, enhanced by the high spatial and temporal resolution and precision of X-band SAR. This study has provided additional insight into the behaviour of groundwater flow in the Perth Basin, through the pattern and magnitude of land surface displacements resulting from the focus on the start and variable progression of the MAR program. The variable spatial extent of the MAR dispersal is likely to be dominated by the location of groundwater extraction bores and heterogeneities in the subsurface geology, including persistent linear features that have not yet been considered in some hydrogeological models.

CRedit authorship contribution statement

A.L. Parker: Conceptualization, Investigation, Writing – original draft, Writing – review & editing. **J.-P. Pigois:** Conceptualization, Writing – original draft. **M.S. Filmer:** Conceptualization, Writing – original draft, Writing – review & editing, Formal analysis. **W.E. Featherstone:** Conceptualization, Formal analysis, Funding acquisition. **N.E. Timms:** Conceptualization, Writing – original draft. **N.T. Penna:** Conceptualization, Formal analysis.

Declaration of Competing Interest

The authors declare that they have no known competing financial interests or personal relationships that could have appeared to influence the work reported in this paper.

Acknowledgements

This paper is published with the permission of the Water Corporation of Western Australia. Earlier parts of this work were supported financially by Australian Research Council linkage project LP140100155, Landgate (the Western Australian geodetic agency), the Western Australian Department of Water, and Curtin University. ALP was the recipient of an Australian Research Council Discovery Early Career Researcher Award (project DE190101389) funded by the Australian Government. We thank: (1) the German Aerospace Centre (DLR) for supplying TerraSAR-X data under science project LAN_1499; (2) Stuart Wilcox, manager of the RTKNetWest network (<http://www.rtknetwest.com.au/>), for providing cGPS data at STIG; (3) NASA JPL for the GipsyX software, satellite orbits and clocks; (4) Geoscience Australia and the International GNSS Service for providing GPS data.

References

- Bell, J.W., Amelung, F., Ferretti, A., Bianchi, M., Novali, F., 2008. Permanent scatterer InSAR reveals seasonal and long-term aquifer-system response to groundwater pumping and artificial recharge. *Water Resources Research* 44 (2), W02407. <https://doi.org/10.1029/2007WR006152>.
- Berardino, P., Fornaro, G., Lanari, R., Sansosti, E., 2002. A new algorithm for surface deformation monitoring based on small baseline differential SAR interferograms. *IEEE Transactions on Geoscience and Remote Sensing* 40 (11), 2375–2383. <https://doi.org/10.1109/TGRS.2002.803792>.
- Bertiger, W., Bar-Sever, Y., Dorsey, A., Haines, B., Harvey, N., Hemberger, D., Heflin, M., Lu, W., Miller, M., Moore, A.W., Murphy, D., Ries, P., Romans, L., Sibois, A., Sibthorpe, A., Szilagyi, B., Vallisneri, M., Willis, P., 2020. GipsyX/RTGx, a new tool for space geodetic operations and research. *Advances in Space Research* 66, 469–489. <https://doi.org/10.1016/j.asr.2020.04.015>.
- Blewitt, G., Hammond, W.C., Kreemer, C., 2018. Harnessing the GPS data explosion for interdisciplinary science. *EOS – Transactions of the American Geophysical Union* 99. <https://doi.org/10.1029/2018EO104623>.
- Brandt, J.T., Sneed, M., Danskin, W.R., 2020. Detection and measurement of land subsidence and uplift using interferometric synthetic aperture radar, San Diego, California, USA, 2016–2018. *Proceedings of the International Association of Hydrological Sciences* 382, 45–49. <https://doi.org/10.5194/piahs-382-45-2020>.
- Bürgmann, R., Rosen, P.A., Fielding, E.J., 2000. Synthetic aperture radar interferometry to measure Earth's surface topography and its deformation. *Annual Review of Earth and Planetary Sciences* 28 (1), 169–209. <https://doi.org/10.1146/earth.2000.28.issue-110.1146/annurev.earth.28.1.169>.
- Castellazzi, P., Schmid, W., 2021. Interpreting C-band InSAR ground deformation data for large-scale groundwater management in Australia. *Journal of Hydrology: Regional Studies* 34, 100774. <https://doi.org/10.1016/j.ejrh.2021.100774>.
- Chaussard, E., Bürgmann, R., Shirzaei, M., Fielding, E.J., Baker, B., 2014. Predictability of hydraulic head changes and characterization of aquifer-system and fault properties from InSAR-derived ground deformation. *Journal of Geophysical Research: Solid Earth* 119 (8), 6572–6590. <https://doi.org/10.1002/jgrb.v119.8.10.1002/2014JB011266>.
- Chaussard, E., Farr, T.G., 2019. A New Method for Isolating Elastic From Inelastic Deformation in Aquifer Systems: Application to the San Joaquin Valley, CA. *Geophys. Res. Lett.* 46 (19), 10800–10809. <https://doi.org/10.1029/2019GL084418>.
- Chaussard, E., Milillo, P., Bürgmann, R., Perissin, D., Fielding, E.J., Baker, B., 2017. Remote sensing of ground deformation for monitoring groundwater management practices: Application to the Santa Clara Valley during the 2012–2015 California drought. *Journal of Geophysical Research: Solid Earth* 122 (10), 8566–8582. <https://doi.org/10.1002/2017JB014676>.
- Chen, J., Knight, R., Zebker, H.A., Schreüder, W.A., 2016. Confined aquifer head measurements and storage properties in the San Luis Valley, Colorado, from spaceborne InSAR observations. *Water Resources Research* 52 (5), 3623–3636. <https://doi.org/10.1002/2015WR018466>.
- Clohesy, S., 2017. Groundwater Chemistry and Isotope Survey, Perth, Western Australia. *Hydrogeological Report Series*. Department of Water, Perth, WA HR370.
- Corbel, S., Schilling, O., Horowitz, F.G., Reid, L.B., Sheldon, H.A., Timms, N.E., Wilkes, P., 2012. Identification and geothermal influence of faults in the Perth metropolitan area, Australia. *Thirty-Seventh Workshop on Geothermal Reservoir Engineering*. Stanford University, California.
- Davidson, W.A., Yu, X., 2008. Perth regional aquifer modelling system (PRAMS) model development: Hydrogeology and groundwater modelling. Western Australia Department of Water, Hydrogeological record series HG 20. Perth, Australia. Accessed online on 14 April 2021: https://www.water.wa.gov.au/data/assets/pdf_file/0015/5280/71802.pdf.
- De Silva, J., Wallace-Bell, P., Yesertener, C., Ryan, S., 2013. *Perth Regional Aquifer Modelling System (PRAMS) v 3.5: Conceptual model*, Hydrogeological report series, Report no. HR334, Department of Water, Government of Western Australia.
- DWER, 2021. *Studying Perth's deep aquifers to improve their management: Findings and recommendations from the Perth Region Confined Aquifer Capacity study*, Hydrogeological Record series report no. 67, Department of Water and Environmental Regulation, Perth. Available on request.

- Farr, T.G., Rosen, P.A., Caro, E., Crippen, R., Duren, R., Hensley, S., Kobrick, M., Paller, M., Rodriguez, E., Roth, L., Seal, D., Shaffer, S., Shimada, J., Umland, J., Werner, M., Oskin, M., Burbank, D., Alsdorf, D., 2007. The Shuttle Radar Topography Mission. *Reviews of Geophysics* 45 (2), RG2004. <https://doi.org/10.1029/2005RG000183>.
- Featherstone, W.E., Penna, N.T., Filmer, M.S., Williams, S.D.P., 2015. Nonlinear subsidence at Fremantle, a long-recording tide gauge in the Southern Hemisphere. *Journal of Geophysical Research: Oceans* 120 (10), 7004–7014. <https://doi.org/10.1002/jgrc.v120.1010.1002/2015JC011295>.
- Filmer, M.S., Williams, S.D.P., Hughes, C.W., Wöppelmann, G., Featherstone, W.E., Woodworth, P.L., Parker, A.L., 2020. An experiment to test satellite radar interferometry-observed geodetic ties to remotely monitor vertical land motion at tide gauges. *Global and Planetary Change* 185, 103084. <https://doi.org/10.1016/j.gloplacha.2019.103084>.
- Finnegan, N.J., Pritchard, M.E., Lohman, R.B., Lundgren, P.R., 2008. Constraints on surface deformation in the Seattle, WA, urban corridor from satellite radar interferometry time-series analysis. *Geophysical Journal International* 174 (1), 29–41. <https://doi.org/10.1111/j.1365-246X.2008.03822.x>.
- Galloway, D.L., Burbey, T.J., 2011. Regional land subsidence accompanying groundwater extraction. *Hydrogeology Journal* 19 (8), 1459–1486. <https://doi.org/10.1007/s10040-011-0775-5>.
- Gambolati, G., Teatini, P., 2015. Geomechanics of subsurface water withdrawal and injection. *Water Resources Research* 51 (6), 3922–3955. <https://doi.org/10.1002/2014WR016841>.
- Gomba, G., Gonzalez, F.R., De Zan, F., 2017. Ionospheric Phase Screen Compensation for the Sentinel-1 TOPS and ALOS-2 ScanSAR Modes. *IEEE Trans. Geosci. Remote Sens.* 55 (1), 223–235. <https://doi.org/10.1109/TGRS.2016.2604461>.
- Hooper, A., Segall, P., Zebker, H., 2007. Persistent scatterer interferometric synthetic aperture radar for crustal deformation analysis, with application to Volcán Alcedo, Galápagos. *Journal of Geophysical Research: Solid Earth* 112 (B7), B07407. <https://doi.org/10.1029/2006JB004763>.
- IPCC, 2007. *Climate Change 2007: Impacts, Adaptation and Vulnerability. Contribution of Working Group II to the Fourth Assessment Report of the Intergovernmental Panel on Climate Change*. Cambridge University Press, Cambridge, UK, 976 pp. *Accessed online on 14 April 2021*.
- Johnston, P.J., Filmer, M.S., Fuhrmann, T., 2021. Evaluation of methods for connecting InSAR to a terrestrial reference frame in the Latrobe Valley, Australia. *Journal of Geodesy* 95, 115. <https://doi.org/10.1007/s00190-021-01560-2>.
- Lambeck, K., 1987. The Perth basin: A possible framework for its formation and evolution. *Exploration Geophysics* 18 (2), 124–128. <https://doi.org/10.1071/EG987124>.
- Lu, Z., Danskin, W.R., 2001. InSAR analysis of natural recharge to define structure of a ground-water basin, San Bernardino, California. *Geophysical Research Letters*, 28 (13), 2661–2664. <https://doi.org/10.1029/2000GL012753>.
- Lyon, T.J., Filmer, M.S., Featherstone, W.E., 2018. On the use of repeat leveling for the determination of vertical land motion: artifacts, aliasing and extrapolation. *Journal of Geophysical Research: Solid Earth* 123 (8), 7021–7039. <https://doi.org/10.1029/2018JB015705>.
- Massonnet, D., Rossi, M., Carmona, C., Adragna, F., Peltzer, G., Feigl, K., Rabautte, T., 1993. The displacement field of the Landers earthquake mapped by radar interferometry. *Nature* 364 (6433), 138–142. <https://doi.org/10.1038/364138a0>.
- McFarlane, D., Stone, R., Martens, S., Thomas, J., Silberstein, R., Ali, R., Hodgson, G., 2012. Climate change impacts on water yields and demands in south-western Australia. *Journal of Hydrology* 475, 488–498. <https://doi.org/10.1016/j.jhydrol.2012.05.038>.
- Neely, W.R., Borsa, A.A., Burney, J.A., Levy, M.C., Silverii, F., Sneed, M., 2021. Characterization of groundwater recharge and flow in California's San Joaquin Valley from InSAR-observed surface deformation. *Water Resources Research*, 57, e2020WR028451. <https://doi.org/10.1029/2020WR028451>.
- Olierook, H.K.H., Timms, N.E., Wellmann, J.F., Corbel, S., Wilkes, P.G., 2015. 3D structural and stratigraphic model of the Perth Basin, Western Australia: Implications for sub-basin evolution. *Australian Journal of Earth Sciences* 62 (4), 447–467. <https://doi.org/10.1080/08120099.2015.1054882>.
- Parker, A.L., Filmer, M.S., Featherstone, W.E., 2017. First results from Sentinel-1A InSAR over Australia: Application to the Perth Basin. *Remote Sensing* 9 (3), 299. <https://doi.org/10.3390/rs9030299>.
- Playford, P.E., Low, G.H., Cockbain, A.E., 1976. *Geology of the Perth Basin, Western Australia. Report 124, Geological Survey of Western Australia: Perth, Australia.*
- Poland, J.F., Ireland, R.L., 1988. *Mechanics of Aquifer Systems. US Geological Survey Professional Paper 497.*
- Reeves, J.A., Knight, R., Zebker, H.A., Schreüder, W.A., Agram, P., Lauknes, T.R., 2011. High quality InSAR data linked to seasonal change in hydraulic head for an agricultural area in the San Luis Valley, Colorado. *Water Resources Research* 47 (12), W12510. <https://doi.org/10.1029/2010WR010312>.
- Sneed, M., Brandt, J.T., Solt, M., 2014. Land subsidence, groundwater levels, and geology in the Coachella Valley, California, 1993–2010. *U.S. Geological Survey Scientific Investigations Report 2014–5075*, [DOI: 10.3133/sir20145075](https://doi.org/10.3133/sir20145075), 62 pp.
- Sneed, M., Brandt, J.T., 2020. Mitigating land subsidence in the Coachella Valley, California, USA: An emerging success story, *Proceedings of the International Association of Hydrological Sciences* 382, 809–813. <https://doi.org/10.5194/piahs-382-809-2020>.
- Teatini, P., Gambolati, G., Ferronato, M., Settari, A.T., Walters, D., 2011. Land subsidence of natural transitional environments by satellite radar interferometry on artificial reflectors. *Journal of Geophysical Research: Earth Surface* 118 (2), 1177–1191. <https://doi.org/10.1002/jgrf.20082>.
- Theis, C.V., 1935. The relation between the lowering of the piezometric surface and the rate and duration of discharge of a well using groundwater storage. *EOS – Transactions of the American Geophysical Union* 16 (2), 519–524. <https://doi.org/10.1029/TR016i002p00519>.
- Timms, N.E., Corbel, C., Olierook, H., Wilkes, P.G., Delle Piane, C., Sheldon, H.A., Alix, R., Horowitz, F.G., Wilson, M.E.J., Evans, K.A., Griffiths, C., Stütenbecker, L., Israni, S., Hamilton, P.J., Esteban, L., Cope, P., Evans, C., Pimienta, L., Dyt, C., Huang, X., Hopkins, J., Champion, D., 2012. Perth Basin Assessments Program, Project 2: Geomodel. *Western Australia Geothermal Centre of Excellence. WAGCoE Report EP122443*, 202 pp. ISBN: 978-0-643-10905-6.
- Timms, N.E., Olierook, H.K., Wilson, M.E., Delle Piane, C., Hamilton, P.J., Cope, P., Stütenbecker, L., 2015. Sedimentary facies analysis, mineralogy and diagenesis of the Mesozoic aquifers of the central Perth Basin, Western Australia. *Marine and Petroleum Geology* 60, 54–78. <https://doi.org/10.1016/j.marpetgeo.2014.08.024>.
- Water Corporation, 2009. *Water forever 50 year plan*. *Accessed on 14 April 2021: <http://www.watercorporation.com.au/-/media/WaterCorp/Documents/Our-Water/Sustainability-and-Innovation/Securing-Supply/Water-forever-50-year-plan.pdf>*.
- Wright, T.J., Parsons, B.E., Lu, Z., 2004. Toward mapping surface deformation in three dimensions using InSAR. *Geophysical Research Letters* 31 (1), 01607. <https://doi.org/10.1029/2003GL018827>.